Environmental Science & Technology

pubs.acs.org/est

Article

Goethite and Hematite Nucleation and Growth from Ferrihydrite: Effects of Oxyanion Surface Complexes

Alireza Namayandeh,* Wei Zhang, Steven K. Watson, Olaf J. Borkiewicz, Nefeli M. Bompoti, Maria Chrysochoou, R. Lee Penn, and F. Marc Michel

Cite This: *Environ. Sci. Technol.* 2024, 58, 5952−5962

Read Online

ACCESS | Metrics & More | Article Recommendations | Supporting Information

ABSTRACT: The presence of oxyanions, such as nitrate (NO_3^-) and phosphate (PO_4^{3-}), regulates the nucleation and growth of goethite (Gt) and hematite (Hm) during the transformation of ferrihydrite (Fh). Our previous studies showed that oxyanion surface complexes control the rate and pathway of Fh transformation to Gt and Hm. However, how oxyanion surface complexes control the mechanism of Gt and Hm nucleation and growth during the Fh transformation is still unclear. We used synchrotron scattering methods and cryogenic transmission electron microscopy to investigate the effects of NO_3^- outer-sphere complexes and PO_4^{3-} inner-sphere complexes on the mechanism of Gt and Hm formation from Fh. Our TEM results indicated that Gt particles form through a two-step model in which Fh particles first transform to Gt nanoparticles and then crystallographically align and grow to larger particles by oriented attachment (OA). In contrast, for the formation of Hm, imaging shows that Fh particles first aggregate and then transform to Hm through interface nucleation. This is consistent with our X-ray scattering results, which demonstrate that NO_3^- outer-sphere and PO_4^{3-} inner-sphere complexes promote the formation of Gt and Hm, respectively. These results have implications for understanding the coupled interactions of oxyanions and iron oxy-hydroxides in Earth-surface environments.

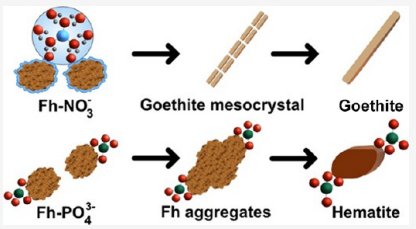

KEYWORDS: *ferrihydrite, oxyanion, transformation, growth, nitrate, phosphate, oriented attachment, dissolution/recrystallization*

INTRODUCTION

Iron oxy-hydroxides, such as ferrihydrite (Fh; $Fe_{1.0}O_{0.67}(OH)_{1.63}$), goethite (Gt; α-FeOOH), and hematite (Hm; α-Fe_2O_3) are pervasive in Earth's surface environments[1−4] and play a significant role in (bio)geochemical element cycling[4−8] due to their high surface area and surface reactivity. Ferrihydrite, in particular, is thermodynamically metastable and, in oxic conditions, undergoes transformation into nanocrystalline Gt and Hm, which can subsequently grow and form larger particles.[9−17] The reduction in accessible surface area and surface reactivity of these iron oxy-hydroxides, resulting from their phase transformation and growth, can influence their interactions with oxyanions like nitrate (NO_3^-) and phosphate (PO_4^{3-}).[18] This, in turn, can impact nutrient availability in soil and water, as well as lead to environmental issues, such as eutrophication,[19] and human health concerns, including preterm birth.[20]

The transformation of Fh into Gt and Hm occurs through two primary mechanisms. In the dissolution/recrystallization pathway, the mass fraction of Gt and Hm increases at the expense of dissolving Fh particles.[14,21] The alternative pathway, known as transformation by interface nucleation, involves solid-state recrystallization through the nucleation of a new phase at the interface between two surfaces.[10,22,23] These mechanisms share similarities with crystal growth processes, specifically coarsening and oriented attachment (OA), respectively.[10]

Oxyanion surface complexes can significantly influence the nucleation and growth mechanisms of Hm and Gt during the Fh transformation. A recent study[24] demonstrated that inner-sphere complexation with oxalate on Fh alters the mechanism of Hm formation, shifting from ion-by-ion growth to near-interface nucleation and growth. Yuwono et al.[25] reported that the strong binding of the organic compound alizarin to Fh inhibits the aggregation of Gt during the Fh transformation. Similarly, oxyanion surface complexes can control the pathway of the Fh transformation into Gt and Hm. Our recent work[26,27] has shown that weak outer-sphere complexes of NO_3^- promote the Gt formation, whereas strong inner-sphere complexes of PO_4^{3-} induce Hm formation. In addition, for oxyanions such as sulfate (SO_4^{2-}), which form a combination of outer- and inner-sphere complexes on Fh, the pathway of Fh transformation can change when one type of surface complexation becomes increasingly dominant. For instance, an increase in the fraction of SO_4^{2-} inner-sphere complexes on Fh with decreasing pH significantly promotes the formation of Hm during the Fh transformation.[26]

Received: November 27, 2023
Revised: February 28, 2024
Accepted: March 7, 2024
Published: March 20, 2024

The oxyanion surface loading on Fh can also influence the rate and pathway of Fh transformation.[27] Previous studies[11,27] have demonstrated that an increase in PO_4^{3-} and arsenate (AsO_4^{-3}) surface loading on Fh enhances Hm formation during the Fh transformation, attributed to the growing presence of inner-sphere surface complexes on Fh. However, extremely high surface loading of PO_4^{3-} and AsO_4^{3-} can inhibit particle aggregation, leading to the complete suppression of the Fh transformation.[27] While these studies[26,27] have shown a correlation between the formation of Gt and Hm with outer-sphere and inner-sphere complexes, respectively, they have not provided mechanistic evidence explaining how oxyanion surface complexes control the nucleation and growth mechanism of Gt and Hm during the Fh transformation.

The Fh transformation often occurs simultaneously with the growth of Gt and Hm, which complicates the study of their individual contributions.[10] To address this challenge, it is necessary to use different characterization methods that can separately investigate the phase transformation and crystal growth. Transmission electron microscopy (TEM) and X-ray diffraction (XRD) are the most commonly used techniques to study Fh transformation and the growth of its transformation products. Cryogenic transmission electron microscopy (cryo-TEM) holds particular importance in understanding the mechanisms of nanoparticle nucleation and growth. This significance arises from the fact that the drying process in conventional TEM sample preparation often leads to nanoparticle aggregation artifacts, whereas cryo-TEM allows the examination of nanoparticles in their true suspension state.

Researchers like Penn and co-workers[16,17,25,28−32] have used TEM and cryo-TEM to investigate crystal growth by OA. They have demonstrated that Gt growth from Fh follows a two-step process: Fh initially transforms to Gt nanoparticles through dissolution/recrystallization and then undergoes OA. In another study,[23] *in situ* TEM was used to examine OA of Fh. This study revealed that during OA, particles engage in direction-specific interactions to achieve a perfect lattice match with neighboring particles. It is worth noting that most of these studies have focused on 6-line rather than 2-line Fh. This preference arises from the fact that 2-line Fh exhibits lower crystallinity and is more susceptible to dissolution compared to 6-line Fh, making it less ideal for studying growth through OA.

While XRD primarily provides information about the bulk properties of particles, it remains a valuable tool for detecting new phases that may form during the Fh transformation. Studies on phase transformation, especially during the transformation of 2-line Fh, have frequently relied on XRD to calculate the Hm/Gt ratio.[12,14,33] However, conducting Rietveld refinement of XRD patterns poses challenges when dealing with poorly crystalline 2-line Fh, especially at early transformation stages.[10] Hence, supplementary characterization techniques are essential to accurately quantify the mass fractions of Gt and Hm.

In recent studies, we have introduced a new method using pair distribution function (PDF) analysis to quantify the abundance of Hm and Gt throughout the Fh transformation.[26,27] PDF analysis, which represents interatomic distances between pairs of atoms and does not necessitate long-range periodicity in their arrangements,[34] offers reasonable accuracy for quantifying the mass fraction of nanosized Fh, Gt, and Hm. By integrating results from PDF and TEM, we gain a unique opportunity to investigate the formation and growth of Gt and Hm during the Fh transformation.

This study examines the influence of adsorbed NO_3^- and PO_4^{3-} on the nucleation and growth of Gt and Hm during the Fh transformation. The objective is to elucidate how oxyanion surface complexes, ranging from weak outer-sphere complexes for NO_3^- to strong inner-sphere complexes for PO_4^{3-}, govern the mechanisms underlying these processes. To the best of our knowledge, this work represents the first systematic investigation of the mechanisms of Gt and Hm nucleation and growth from Fh in the presence of different oxyanion surface complexes. Our findings serve to characterize the respective contributions of phase transformation and crystal growth during the Fh transformation to the formation of Gt and Hm, shedding light on how oxyanions influence these mechanisms.

MATERIALS AND METHODS

Sample Preparation and Adsorption Experiment. 2-line Fh was synthesized following a procedure adopted from Schwertmann and Cornell.[2] While stirring, the pH of 0.2 M $Fe(NO_3)_3$ (ACS grade, Fisher Scientific) solution was adjusted to 7.5 ± 0.2 using a 2 M NaOH solution within 25 min. The resulting suspensions were then centrifuged and dialyzed in a water bath to remove the excessive salts. The density of the samples was measured by drying 2 mL of Fh suspension under the hood for 24 h and then weighing the resulting solids. The measured density was then used to calculate the 5 g/L of Fh needed for the batch adsorption experiments. For the NO_3^--adsorption experiment (FhN), 100 mM $NaNO_3$ was mixed with the Fh suspension in 50 mL centrifuge tubes. For the PO_4^{3-} experiment (FhP), 0.6 mM Na_2HPO_4 in the background of 100 mM $NaNO_3^-$ was used. $NaNO_3^-$ was used as a background electrolyte in the FhP experiment to adjust the ionic strength to 0.1 M, similar to the ionic strength used in the FhN experiment. The molar (M) ratios of PO_4^{3-}/Fh and NO_3^-/Fh were 0.012 and 1.9, respectively. These surface loadings were chosen to observe the impacts of each oxyanion while still allowing the Fh transformation to reach a steady state. Additionally, we prepared a set of Fh samples without oxyanion as the control Fh.

To achieve equilibrium in the adsorption reactions, the pH of all samples was adjusted to 5.5 ± 0.2 using 1 M HNO_3 and NaOH and then incubated at 25 °C for 24 h.[35−37] This pH level, relevant to many soils (e.g., paddy soils) and aqueous environments,[38−40] is ideal for studying the mechanism of Gt and Hm formation from Fh. At this pH, both Gt and Hm can form concurrently.[12] Moreover, the adsorption of PO_4^{3-} and NO_3^- can effectively occur at this pH through distinct oxyanion surface complexes,[26,27] enabling a thorough examination of the impacts of oxyanion surface complexes on the formation of Gt and Hm from Fh.

The samples were centrifuged for 10 min at 7000 rcf to separate solids from the solution. The supernatant was then filtered using a 0.22 μm centrifuge filter, and high-performance liquid chromatography−ion conductivity (IC) was used to measure the concentration of PO_4^{3-} and NO_3^-. This allowed us to calculate the amounts of PO_4^{3-} and NO_3^- adsorbed onto the Fh surface.

Surface complexation modeling was used to predict the type of PO_4^{3-} binding on the Fh surface, with further details provided in Text S1 and Table S1. Additionally, we used *in situ* attenuated total reflectance Fourier transform infrared spec-

https://doi.org/10.1021/acs.est.3c09955
Environ. Sci. Technol. 2024, 58, 5952−5962

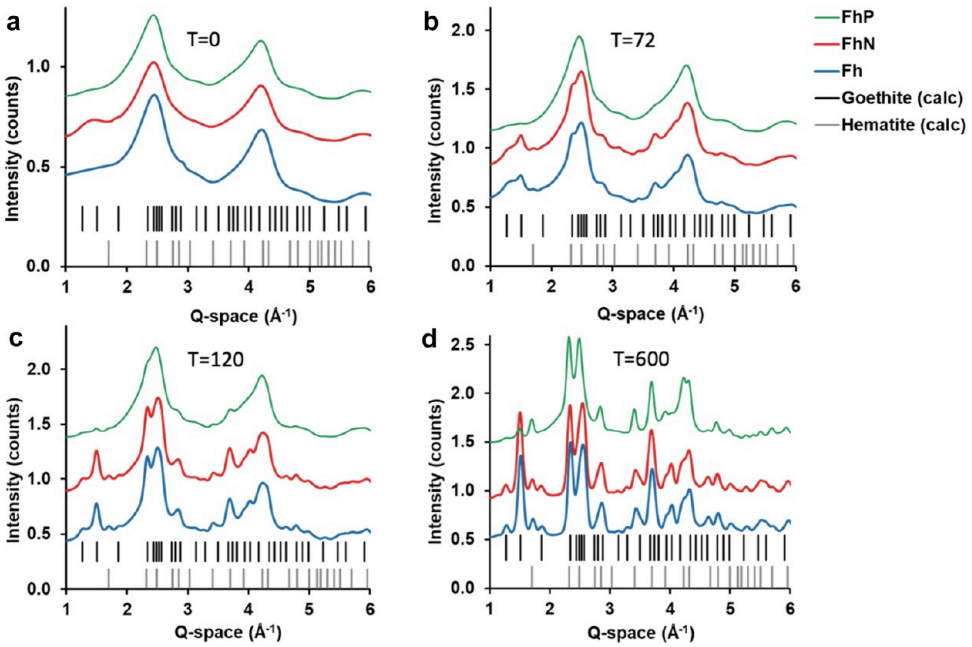

Figure 1. Synchrotron powder X-ray diffraction data for selected samples at (a) 0, (b) 72, (c) 120, and (d) 600 h of aging. The control Fh sample reaches a steady state condition at 600 h, and this time point was selected to enable a comparison of FhN and FhP samples with the control Fh under steady-state conditions.

troscopy (ATR-FTIR) to investigate NO_3^- complexation on Fh. Text S2 provides the details of the ATR-FTIR method.

Transformation Experiment. For the aging experiments, the samples and control underwent centrifugation at 7000 rcf for 10 min to separate solids from the solution. Subsequently, the supernatant was carefully decanted, and the pH of the resulting pastes was buffered by adding a quantity of 0.4 M MES ($C_6H_{13}NO_4S$). The paste was mixed with the buffer solution by shaking. Further adjustment of the pH to 5.5 ± 0.2 was achieved using 2 M NaOH. The prepared samples were transferred into 10 mL of high-density polyethylene (HDPE) plastic leakproof opaque bottles.

These samples were then placed inside a sealed water bath within a mechanical convection laboratory oven (Thermo Scientific Heratherm) and aged at 70 ± 1.5 °C. This temperature was chosen to accelerate the rate of Fh transformation, enabling the observation of Gt and Hm formation within a reasonable laboratory experiment time frame. Additionally, this temperature allowed for the concurrent formation of Gt and Hm.[12] Subsequently, the samples were periodically removed from the oven at various time points (0, 24, 48, 72, 120, 168, 240, 360, 600, 888, and 1200 h) and subjected to centrifugation for 10 min at 7000 rcf to recover the solids. The solution phase was filtered using 0.22 μm centrifuge filters, and the filtered solution was analyzed for PO_4^{3-} and NO_3^- using IC.

Synchrotron High-Energy X-ray Scattering. The aged samples were characterized to identify and quantify the Fh transformation products. To prepare these samples, the recovered pastes were air-dried at room temperature in a flowing atmosphere for 24 h, then crushed into fine powders using a mortar and pestle. These powders were loaded in 1 mm OD (outside diameter) polyimide capillaries and analyzed using synchrotron high energy X-ray scattering at beamline 11-ID-B at the Advanced Photon Source, Argonne National Laboratory. Raw scattering data were processed using GSAS-II, and background subtraction, as well as the conversion of reciprocal-space data into real-space PDFs, was performed using xPDFsuite[41] with a max Q-space of 24−25 $Å^{-1}$ for the Fourier transform.

The abundance of Fh and the transformation products was determined through linear combination fitting (LCF) of the PDF data. PDF provides interatomic distances between pairs of atoms specific to each mineralogical phase, making LCF an ideal method for quantifying the proportions of Fh, Gt, and Hm in mixed phases. Synthetic 2-line Fh, Gt, and Hm reference PDFs were fitted for each sample, and LCF was conducted from 0 to 20 Å using WinXAS.[42] The final abundance sum was normalized to 100%, and phase concentrations at different time points were calculated as percentages.

Cryogenic Transmission Electron Microscopy. Cryo-TEM experiments were conducted to directly observe the transformation of Fh to Gt and Hm. Samples were prepared by pipetting three microliters of fresh and aged Fh suspension onto a 400-mesh glow discharged ultrathin carbon grid (Ted Pella, Inc.). The grid was blotted with filter paper and plunged into liquid ethane to form vitreous ice. The frozen grid was then imaged using an FEI Tecnai G^2 F30 TEM operating at 300 kV, equipped with a cryogenic sample stage and a Gatan Summit K2 direct electron detector camera (Gatan, Inc.) for imaging.

RESULTS AND DISCUSSION

Oxyanion Surface Complexes and Adsorption Behavior. The details of PO_4^{3-} and NO_3^- surface complexes on the Fh surface and their adsorption behaviors during the Fh transformation have been extensively discussed by Namayandeh et al.[26,27] The surface complexation modeling revealed that PO_4^{3-} predominantly forms bidentate inner-sphere complexes on Fh (Table S1). We attempted surface complexation modeling for both oxyanion adsorptions, but it proved more

https://doi.org/10.1021/acs.est.3c09955
Environ. Sci. Technol. 2024, 58, 5952−5962

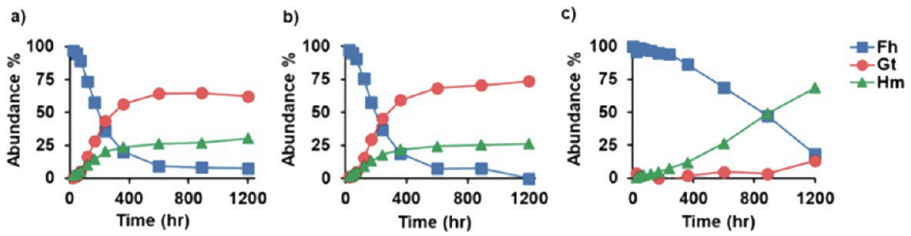

Figure 2. Abundances of Fh, Gt, and Hm with time for (a) control Fh, (b) NO_3^--adsorbed Fh, and (c) PO_4^{3-}-adsorbed Fh. The error bars correspond to standard error (n = 3). Error bars are smaller than the symbol.

suitable for calculating inner-sphere complexation and could not accurately predict outer-sphere complexes. As a result, we turned to ATR-FTIR to examine NO_3^- complexation. ATR-FTIR analysis exhibited a broad peak at 1365 cm^{-1}, attributed to NO_3^- outer-sphere complexes (Figure S1), consistent with previous studies.[4,43−51] Additionally, the results indicated that PO_4^{3-} was entirely adsorbed on Fh (0.6 mM) and was not released into the solution during the Fh transformation, as no PO_4^{3-} was detected in the solution phase throughout the aging experiment. In contrast, IC analysis revealed that out of the initial 100 mM NO_3^- concentration, approximately 60.9 ± 0.3 mM NO_3^- was adsorbed, with approximately 5.8 mM desorbing from the Fh surface with aging. Weak outer-sphere complexes of NO_3^- cannot compete with strong inner-sphere complexes of PO_4^{3-}, and their adsorption on the Fh surface in the FhP experiment was insignificant.

Phosphate inner-sphere and NO_3^- outer-sphere complexation reactions on Fh are as follows:

$$2{\equiv}FeOH + 2H^+ + PO_4^{3-} \leftrightarrow ({\equiv}FeO)_2PO_2^{2-} + 2H_2O$$

$${\equiv}FeOH_2 + NO_3^- \leftrightarrow [{\equiv}FeOH_2 - NO_3^-]$$

According to these reactions, the adsorption of PO_4^{3-} through inner-sphere complexes results in the desorption of water, while NO_3^- maintains the degree of hydration on the Fh surface. Previous density function theory (DFT) calculations[27] showed that PO_4^{3-} is adsorbed on the Fh surface by displacing two H_2O molecules. Additionally, prior to adsorption, Fe-(OH)-Fe is H-bonded to an H_2O molecule in aqueous solution and HPO_4^{3-}, while after adsorption, Fe-(OH)-Fe is H-bonded to an O molecule in PO_4^{3-}, further dehydrating the Fh surface. A stronger solvation effect (i.e., greater dehydration) occurs during the formation of inner-sphere complexes compared to outer-sphere species, leading to water desorption during inner-sphere complexation.[52−54] This is because the Gibbs free energy (ΔG) of hydration is highly negative for inner-sphere complexation, while for outer-sphere complexes, $\Delta G_{deh} > 0$.[36] The ionic potential (IP = charge (Z)/radius (r)) of NO_3^- (0.50) is significantly smaller than that of PO_4^{3-} (1.25), and unlike PO_4^{3-}, NO_3^- lacks the strength to displace water molecules from the Fh surface.[26,27,55] This leads to the formation of NO_3^- outer-sphere complexes.

Products, Pathway, and Rate of Fh Transformation. Synchrotron powder XRD was used to identify the products of the Fh transformation. Figure 1 shows the measured intensity vs Q-space ($Q = \frac{4\pi \sin\theta}{\lambda}$) for all the samples, indexed with the calculated structures of Gt and Hm. The crystallinity of the samples increased with aging, but their crystallization progress differed in the presence of NO_3^- and PO_4^{3-} compared to the control Fh. Phosphate-adsorbed samples (FhP) showed slower transformation progress than the control Fh and FhN samples. Figure S2 illustrates synchrotron powder XRD for the samples at the end of the aging experiments (T = 1200 h). Synchrotron total scattering data were converted to real-space PDFs and the LCF was analyzed to quantify the fractions of the newly formed phases (Figure 2). The PDF data is presented in Figure S3. At the end of the experiments (t = 1200 h), the Gt fraction was higher for FhN (73.63 ± 0.18%) compared to the control Fh (62.2 ± 0.01%). The lowest Gt fraction was observed for Fh aged with adsorbed PO_4^{3-} (13.4 ± 0.18). The Hm fraction decreased from 30.3 ± 0.13% for control Fh to 26.4 ± 1.0% for FhN but significantly increased to 68.8 ± 0.56% for FhP. These results suggest that NO_3^- promotes Gt formation, whereas PO_4^{3-} promotes Hm formation.

We have recently developed a kinetic model that describes the formation of Gt and Hm during the Fh transformation.[26,27] Details regarding the derivation and calculation of this rate model are provided in Text S3 and Figure S4. We used this rate model to calculate the rates of Gt and Hm formation in the presence of NO_3^- and PO_4^{3-}, as shown in Figure S5. To illustrate the specific impacts of NO_3^- and PO_4^{3-} on the rates of Gt and Hm formation, we subtracted the rate of the control samples from that of the NO_3^- and PO_4^{3-} adsorbed samples, resulting in the differential rate (Figure 3). The dashed line in

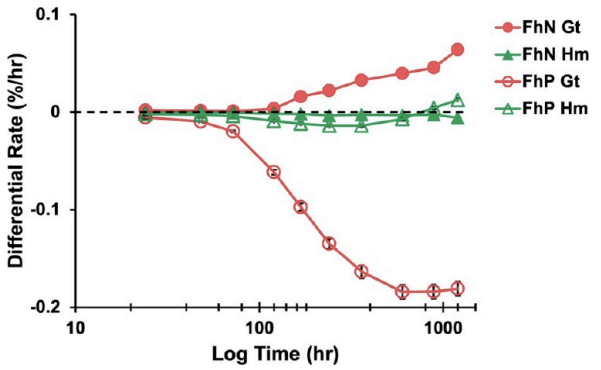

Figure 3. Differential rate of Gt and Hm formation for NO_3^--adsorbed Fh and PO_4^{3-}-adsorbed Fh calculated by subtracting the rates of the Fh control. The dashed line corresponds to the rates of Gt and Hm formation in the control Fh. The x-axis was presented on a logarithmic scale to allow for visualization of the early stage of transformation.

Figure 3 represents the rate of control Fh, with values greater than or smaller than zero, indicating a faster or slower rate of transformation relative to the control, respectively. The results for the first 72 h showed that the differential rate of Gt formation was relatively zero and similar to that of control Fh in the presence of NO_3^-. However, after 72 h, the differential rate of Gt formation progressively increased for the FhN sample. In contrast, the presence of PO_4^{3-} caused a significant

https://doi.org/10.1021/acs.est.3c09955
Environ. Sci. Technol. 2024, 58, 5952−5962

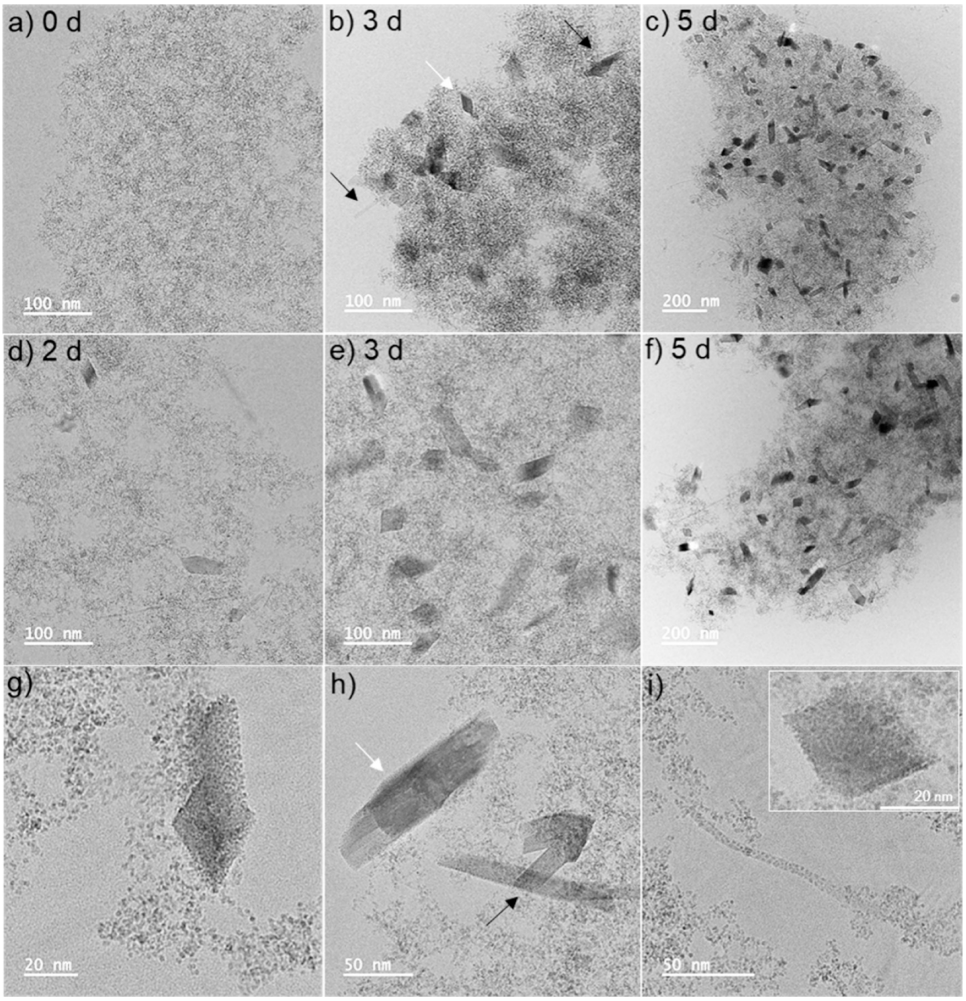

Figure 4. TEM imaging. (a) Fresh Fh material at day 0 for control Fh, (b) acicular Gt (black arrows) and rhombohedral Hm (white arrow) particles at day 3 for control Fh, (c) Gt and Hm particles at day 5 for control Fh. (d–f) Gt and Hm particles from day 2 to 5 for NO_3^--adsorbed Fh, (g) growth of Gt on Hm particles, forming epitaxial twins (control Fh; day 3), (h) Gt twin pieces (white arrow) and dendritic twins (black arrow) forming by nucleation of a Gt particle on the surface of another Gt crystal (FhN; day 5), and (i) Gt mesocrystals and Hm particles (inset) formed from small primary subunits (control Fh; day 3). Features in panels (g–i) are frequently seen in the aged control Fh and NO_3^--adsorbed samples across different time points.

decrease in the differential rate of Gt formation beyond ~24 h, indicating that NO_3^- promotes Gt formation, while PO_4^{3-} suppresses it.

For FhN, the differential rate of Hm formation was nearly zero and similar to control Fh in the presence of NO_3^-, with only a slight decrease observed after 1000 h. Conversely, for FhP, the differential rate of Hm formation remained constant at zero for up to 72 h until approximately 360 h, after which it exhibited a progressively accelerating trend until the end of the experiment, surpassing zero. These findings suggest that NO_3^- has minimal impact on Hm formation, while the presence of PO_4^{3-} initially suppresses Hm formation, but it eventually starts to promote it over time.

Particle Shape and Aggregation State. To investigate the mechanism of Gt and Hm formation from Fh, we imaged samples using Cryo-TEM at the onset of Fh transformation to capture all changes from Fh to intermediate phases and to the final products of the transformation. Cryo-TEM images showed an increase in both Hm and Gt content with aging for both control Fh and FhN (Figure 4a–f). In the fresh samples, the Fh aggregates consisted of fractal-like particles with no evidence of the presence of Gt and Hm (Figure 4a). The observed increase in the contrast of the Fh aggregates over time (Figure 4a–f) suggests an increase in the crystallinity of the primary particles with aging.[10] Acicular and nanorod-shaped particles, consistent with the reported morphology of Gt,[30,56−58] were observed in both the aged control Fh and FhN samples (Figure 4b; black arrow). Additionally, Hm particles with rhombohedral morphology were observed in the same samples (Figure 4b; white arrow).[10,58] Interestingly, Figure 4g shows a close spatial relationship between Gt and Hm in the aged samples, suggesting the growth of Gt on the surface of Hm, a morphology consistent with epitaxial twinning.[2] This occurs due to similarities in the interplanar spacings of Gt and Hm, inducing heterogeneous nucleation and growth.[2,59] Furthermore, Figure 4h provides evidence of twinned Gt particles (white arrow) and dendritic twins (black arrow), consistent with previous reports.[59]

Higher image magnification shows that Gt and Hm consist of many small subunits (Figure 4g, i). The uniform contrast of these subunit particles suggests a similar crystallographic orientation consistent with OA.[10] The aggregation-based crystallization pathway is further supported by the formation of Gt mesocrystals (Figure 4i), where Gt nanocrystals exhibit

https://doi.org/10.1021/acs.est.3c09955
Environ. Sci. Technol. 2024, 58, 5952−5962

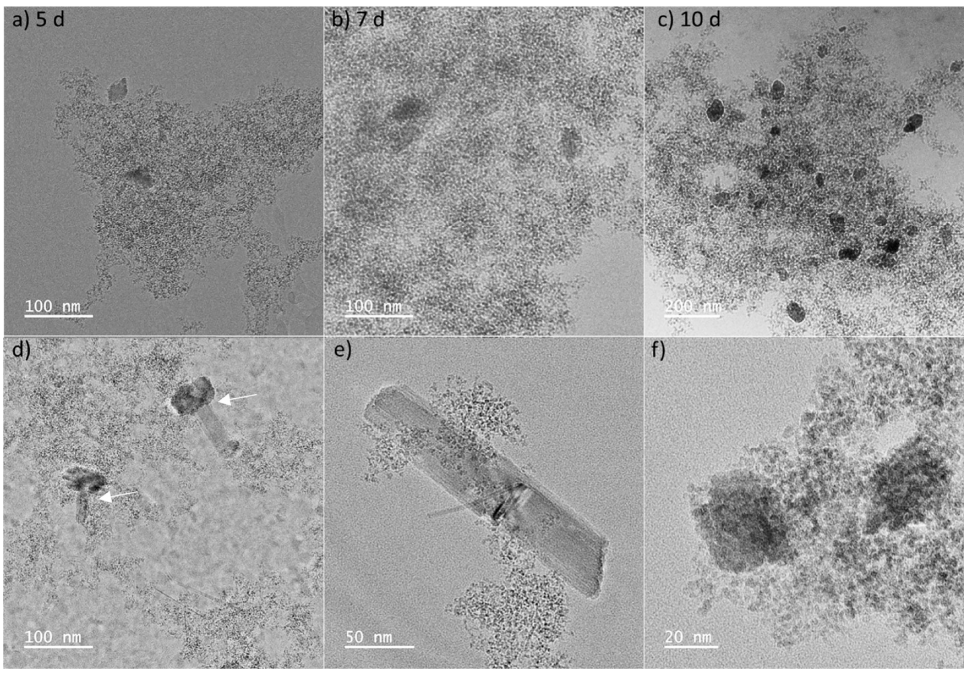

Figure 5. TEM imaging of PO_4^{3-}-adsorbed samples. (a–c) Time-resolved TEM showing more particles formed with aging from day 5 to 10; Hm particles were deformed compared with control and NO_3^--adsorbed Fh, (d) growth of Gt particles on Hm, forming epitaxial twins (arrows) (day 10), (e) large acicular Gt particle (day 7) and (f) two Hm-like aggregates formed of small primary subunits (day 5).

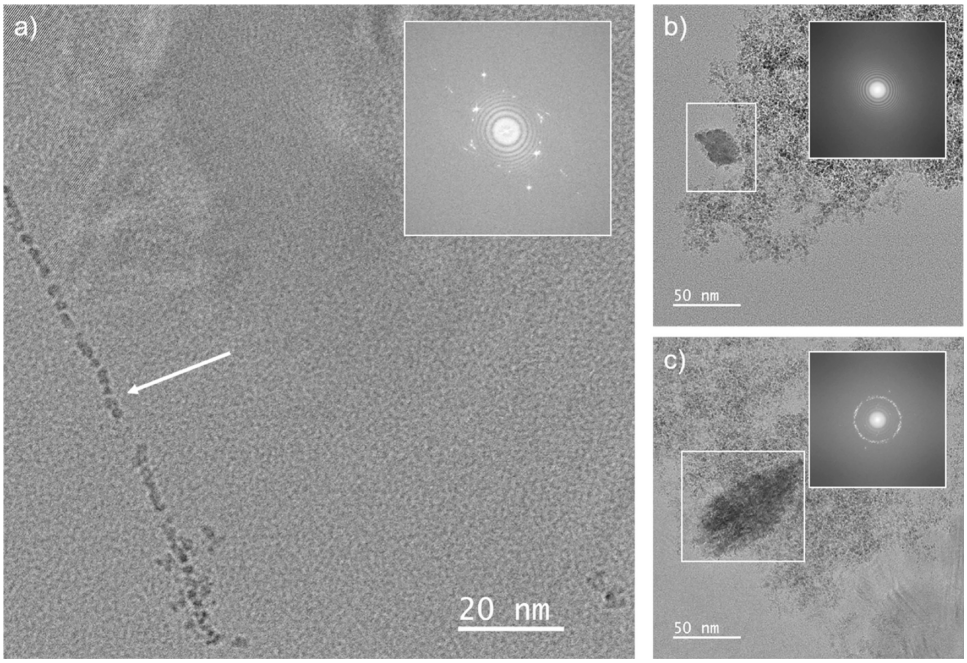

Figure 6. (a) Gt mesocrystals in NO_3^--adsorbed samples after 3 days of aging. Fast Fourier transform (inset) shows that these particles are crystalline. (b) Hm-like aggregates in PO_4^{3-}-adsorbed samples after 5 days of aging. Fast Fourier transform (inset) shows that the samples have not crystallized to Hm yet. (c) Hm-like aggregates in PO_4^{3-}-adsorbed samples after 10 days of aging. Fast Fourier transform (inset) shows that this particle is more crystalline compared to the day 5 sample.

crystallographic alignment but are not attached to any coherent crystalline material.

Phosphate adsorption had a significant impact on the morphologies of Gt and Hm during the Fh transformation. Cryo-TEM showed limited evidence of Hm and Gt formation from 0 to 5 days in the presence of PO_4^{3-} (Figure 5a–c), which is consistent with our scattering results for the same samples. The contrast of primary particles increased on days 7 and 10, indicating the formation of more crystalline products (Figure 5b,c). Aging in the presence of PO_4^{3-} resulted in different Hm morphologies compared to the control Fh and FhN samples. Phosphate adsorption deformed the Hm rhombohedral observed in control Fh and led to the formation of new shapes, such as hexagonal, pseudorhombohedral, or irregular. As expected, based on the scattering results, the abundance of Gt was lower for the FhP samples compared with

https://doi.org/10.1021/acs.est.3c09955
Environ. Sci. Technol. 2024, 58, 5952–5962

the control Fh, although some particles were evident (Figure 5d,e). Single acicular particles were the most common Gt morphology, with sizes up to ~200 nm in length (Figure 5e). Epitaxial twins were also identified (Figure 5d). Twin pieces and dendritic twins were not common.

Mechanism of Gt and Hm Formation. *Impact of NO_3^- and Gt Formation.* Nitrate induced the formation of Gt over Hm. The adsorption of NO_3^- through outer-sphere complexes on Fh can maintain the degree of hydration on the surface of Fh. Additionally, the degree of hydration may increase on the surface through the exchange of NO_3^- hydration,[60,61] including hydroxyl and oxygen,[36] at pH 5.5 ± 0.2 used in this work. We recently proposed that this may promote the dissolution/recrystallization pathway of Fh transformation.[26] The TEM results showed the same Gt and Hm morphologies for both the control Fh and FhN samples, indicating that NO_3^- did not change the shape of Gt and Hm particles. This seems reasonable because NO_3^- forms weak outer-sphere complexes on Fh, where there is no direct contact between NO_3^- and the surface.[26] Cornell and Giovanoli[59] showed that epitaxial twins are formed when dissolution/recrystallization slightly outweighs aggregation pathways.[59] However, if dissolution prevails (e.g., at pH > 12), other types of twins are formed. Twin pieces and dendritic twins were common in the control Fh and FhN samples (Figure 4h), suggesting that dissolution/recrystallization was the dominant mechanism of Gt formation.

The presence of Gt mesocrystals suggests that aggregation and crystallization via OA were also important in the transformation of Fh to large Gt particles for the control Fh and FhN. Yuwono et al.[31] showed the two-step formation of Gt mesocrystals in which the Fh particles initially transform to small Gt particles, and then the resulting particles align crystallographically to form Gt mesocrystals. In another study, Burleson and Penn[16] showed that phase transformation from Fh to Gt occurs through dissolution/recrystallization, while OA dominates the growth of Gt nanodots to nanorods. Figure 6a shows Gt mesocrystals and the corresponding fast Fourier transform (FFT) that indicates that these small primary units were already transformed to crystalline products. This suggests that Gt nanoparticles formed from Fh, and then crystallography aligned and grew through OA. Our results agree with the two-step model that both dissolution/recrystallization and OA pathways were involved in the Gt formation. In addition, it is consistent with our hypothesis that maintaining the degree of hydration through NO_3^- outer-sphere complexes may be responsible for the higher rate of Gt formation for FhN samples.

Impact of PO_4^{3-} on Hm Formation. Phosphate significantly suppressed the formation of Gt and favored the formation of Hm. We attribute these effects to the formation of inner-sphere PO_4^{3-} complexes that displace water (i.e., OH_2 and OH^-), thus suppressing the dissolution and recrystallization pathway. This is supported by the significant decrease in Gt abundance in the presence of PO_4^{3-}, which is consistent with previous studies indicating that the structure and degree of hydration can control the size and shape of Hm nanoparticles.[33,62] Also, Torrent and Guzman[63] showed that the degree of hydration played a significant role in the transformation of Fh, with a lower degree of hydration decreasing the rate of Fh transformation and favoring Hm over Gt formation, which aligns with our results showing that PO_4^{3-} promotes Hm formation.

The presence of PO_4^{3-} distorted the rhombohedral morphology of Hm, but it did not change the shape of the acicular Gt particles. This observation may suggest that Gt was formed in the solution phase, confirming dissolution/precipitation as the primary pathway for Gt formation. The lower rate of Gt formation and the absence of twin pieces and dendritic twins suggest that dissolution and recrystallization were not dominant during Fh transformation in the presence of PO_4^{3-}.

The mechanism of Hm and Gt formation differed during the Fh transformation in the absence and presence of oxyanions. Hematite particles are composed of many small subunits, suggesting that Hm was also formed through a two-step process, as reported by Soltis et al.[10] However, whether phase transformation occurred through dissolution/recrystallization has yet to be understood. Figure 6b shows Fh aggregates after 5 days of aging. Although these aggregates have a shape similar to that of Hm, their corresponding FFT showed that they are not yet crystalline. However, their crystallinity increased on day 10, as shown in Figure 6c. This suggests that unlike Gt, Hm particles formed after aggregation of primary Fh particles. In addition, the deformed shape of Hm particles suggests that PO_4^{3-} was present on the Fh surface during the transformation of primary units to Hm particles. The adsorption of ligands such as PO_4^{3-} on certain faces suppresses their growth in that direction and creates an irregularity in the shape of Hm crystals.[2] Also, the suppression of Gt formation suggests that the dissolution-recrystallization pathway was not dominant during the Fh transformation for FhP samples at these experimental conditions. Therefore, we propose that primary Fh particles aggregated and then underwent a transformation to Hm, which involves interface nucleation as proposed by Li et al.[23] Hematite particles nucleate at the interface between different Fh surfaces and propagate through the remaining primary particles through solid-state recrystallization.[22] It is noteworthy that our data cannot completely rule out the simultaneous occurrence of other pathways that may also control the Fh transformation to some extent. For example, some particles may assemble before or after the phase transformation or dissolution/recrystallization may precipitate some Hm particles in the dimpled surface of large Hm particles.

Phosphate adsorption can facilitate OA by removing water from the interfaces and decreasing positive charges, thereby reducing particle−particle repulsion on the surface. This is in agreement with a previous study[25] and Derjaguin, Landau, Verwey, and Overbeek (DLVO) theory, which shows that the rate of OA increases with decreasing surface protonation.[17,30,32,64] Although PO_4^{3-} promotes the formation of Hm, a higher PO_4^{3-} surface loading can inhibit the Fh transformation, as shown by Namayandeh et al.[27] High surface loading of ligands such as PO_4^{3-} can occupy the interfaces between adjoining Fh particles, suppressing aggregation (i.e., interface nucleation), and inhibiting small subunits from forming larger particles.[25,58] In addition, extreme surface dehydration through PO_4^{3-} inner-sphere complexes removes the minimum degree of water needed to nucleate new phases. In this work, we used a relatively low surface loading of PO_4^{3-} (0.012 PO_4^{3-}/Fh molar ratio) to ensure the Fh transformation reaches completion, and both Gt and Hm can still form.

The present work provides mechanistic information about how oxyanion surface complexes control the nucleation and growth of Gt and Hm during the Fh transformation. We

https://doi.org/10.1021/acs.est.3c09955
Environ. Sci. Technol. 2024, 58, 5952−5962

demonstrated that Fh transforms to Gt and Hm primarily through dissolution/recrystallization and dehydration/aggregation pathways, respectively, with NO_3^- outer sphere complexes promoting Gt and PO_4^{3-} inner-sphere complexes Hm formation. Figure 7 shows a simplified schematic of the mechanism of Gt and Hm formation from Fh precursors in the presence of oxyanions. We propose that the degree of hydration on the Fh surface, regulated by oxyanion surface complexes, is the main factor controlling the rate and pathway of Fh transformation.

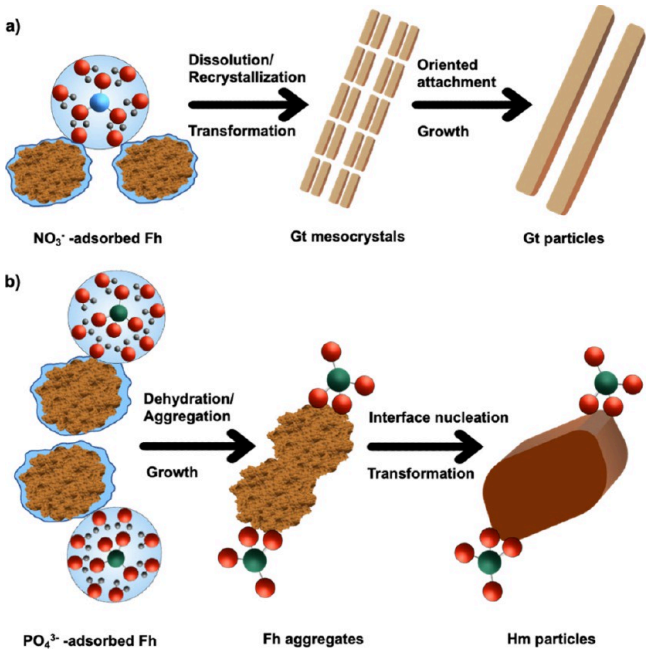

Figure 7. Simplistic schematic of the impact of oxyanion surface complexes on the nucleation and growth of Gt and Hm during the Fh transformation. (a) NO_3^- outer-sphere complexes maintain the hydration on the Fh surface and promote the dissolution/recrystallization pathway, forming Gt particles. These small Gt nanodots crystallographically align, form Gt mesocrystals, and then grow into Gt rods. (b) PO_4^{3-} inner-sphere complexes dehydrate the Fh surface, which promotes the aggregation of Fh particles. The Fh aggregates then transform to Hm through the interface nucleation.

IMPLICATIONS

Due to the increasing consumption of nitrogen and phosphorus in the forms of fertilizers in agriculture,[65,66] understanding the processes controlling the mobilization of these nutrients in aqueous environments has become more critical. This is because the high concentration of PO_4^{3-} and NO_3^- causes detrimental environmental problems such as the eutrophication of surface water.[19] Previous studies have shown that under certain chemical conditions, such as in oxidative environments and acidic to intermediate pH levels, Fh, which is widespread in aquatic environments, can immobilize PO_4^{3-} and NO_3^-, primarily through surface complexation reactions.[26,47,67] However, Fh is thermodynamically metastable and transforms to larger and more crystalline Fe (oxy)-hydroxides such as Gt and Hm.[10−12,68,69] This process can decrease the surface area and reactive sites on the Fh surface, as well as dissolve Fh particles during transformation, which may result in the release of PO_4^{3-} and NO_3^- into the water from the Fh surface.[26] Our results showed that NO_3^- was released into solution while PO_4^{3-} remained on the surface during the Fh transformation. This was attributed to the weaker binding of NO_3^- on Fh and the higher dissolution of Fh primary particles in the presence of NO_3^- during Fh transformation compared to that of the PO_4^{3-}-adsorbed Fh. We also showed that these oxyanions impact the nucleation and growth of Gt and Hm during Fh transformation by forming distinct surface complexes. We showed that more Gt is formed in the presence of NO_3^-. This is attributed to the maintaining hydration on the Fh surface through NO_3^- outer-sphere complexes, which induced the dissolution/recrystallization. Results showed that Gt was formed in two steps: Fh particles first transformed to Gt through dissolution/recrystallization, and then crystallography aligned and grew by OA to larger Gt particles. In addition, results showed that the Gt formation was suppressed, and more Hm formed in the presence of the adsorbed PO_4^{3-}. We suggested that PO_4^{3-} dehydrates the Fh surface through inner-sphere complexes, suppresses the dissolution−crystallization pathway, and promotes interface nucleation, which involves aggregation. This was evidenced by cryo-TEM results showing that Fh particles first aggregated and then transformed to Hm particles through interface nucleation. This work introduces a new combination of characterization methods that allow the study of phase transformation and crystal growth of iron oxyhydroxides and the effects of oxyanion on these mechanisms.

ASSOCIATED CONTENT

Supporting Information

The Supporting Information is available free of charge at https://pubs.acs.org/doi/10.1021/acs.est.3c09955.

Text S1. Surface complexation model. Text S2. *In situ* attenuated total reflectance Fourier transform infrared spectroscopy (ATR-FTIR). Text S3. Rate law derivation. Table S1. Surface complexation reactions, equilibrium constants, and plane charge distribution. Figure S1. ATR-FTIR spectra of NO_3^- adsorbed on Fh at pH 5.5 ± 0.2. Figure S2. Synchrotron powder X-ray diffraction data for samples at 1200 h of aging. Figure S3. PDF data for samples at 0, 240, 360, and 600 h of aging. Figure S4. The ln Fh concentration vs time for control Fh, NO_3^- adsorbed Fh, and PO_3^{3-} adsorbed Fh. Figure S5. The rate of Gt and Hm formation for control Fh, NO_3^- adsorbed Fh, and PO_3^{3-} adsorbed Fh (PDF)

AUTHOR INFORMATION

Corresponding Author

Alireza Namayandeh − *Department of Geosciences, Virginia Tech, Blacksburg, Virginia 24061, United States; Department of Earth System Science, Stanford University, Stanford, California 94305, United States;* orcid.org/0000-0003-2942-3245; Email: arnama@stanford.edu

Authors

Wei Zhang − *Department of Diagnostic and Biological Sciences, University of Minnesota, Minneapolis, Minnesota 55455, United States*

Steven K. Watson − *Department of Geosciences, Virginia Tech, Blacksburg, Virginia 24061, United States*

Olaf J. Borkiewicz − *Advanced Photon Source, Argonne National Laboratory, Lemont, Illinois 60439, United States*

https://doi.org/10.1021/acs.est.3c09955
Environ. Sci. Technol. 2024, 58, 5952−5962

Nefeli M. Bompoti − *Department of Civil and Environmental Engineering, University of Massachusetts, Dartmouth, Massachusetts 02747, United States; Department of Civil and Environmental Engineering, University of Connecticut, Storrs, Connecticut 06269, United States;* orcid.org/0000-0003-2799-188X

Maria Chrysochoou − *Department of Civil and Environmental Engineering, University of Connecticut, Storrs, Connecticut 06269, United States*

R. Lee Penn − *Department of Chemistry, University of Minnesota, Minneapolis, Minnesota 55455, United States;* orcid.org/0000-0002-9610-9507

F. Marc Michel − *Department of Geosciences and Division of Nanoscience, Academy of Integrated Science, Virginia Tech, Blacksburg, Virginia 24061, United States;* orcid.org/0000-0003-2817-980X

Complete contact information is available at: https://pubs.acs.org/10.1021/acs.est.3c09955

Notes

The authors declare no competing financial interest.

■ ACKNOWLEDGMENTS

F.M.M. gratefully acknowledges the financial support provided by the National Science Foundation through CAREER-1652237 and the Virginia Tech National Center for Earth and Environmental Nanotechnology Infrastructure ("Nano-Earth", NSF Cooperative Agreement 1542100). This research used resources of the Advanced Photon Source, a US Department of Energy (DOE) Office of Science User Facility operated for the DOE Office of Science by Argonne National Laboratory under Contract No. DE-AC02-06CH11357. Also, this research was partly funded by the Geological Society of America Graduate Student Research Grant. Cryo-TEM was carried out in the Characterization Facility at the University of Minnesota, which receives partial support from the NSF through the MRSEC (award number DMR-2011401) and the NNCI (award number ECCS-2025124) programs.

■ REFERENCES

(1) Jolivet, J. P.; Chanéac, C.; Tronc, E. Iron Oxide Chemistry. From Molecular Clusters to Extended Solid Networks. *Chem. Commun.* **2004**, No. 5, 481−483.

(2) Schwertmann, U.; Cornell, R. M. *Iron Oxides in the Laboratory*; Wiley: New York,2008.

(3) Jambor, J. L.; Dutrizac, J. E. Occurrence and Constitution of Natural and Synthetic Ferrihydrite, a Widespread Iron Oxyhydroxide. *Chem. Rev.* **1998**, *98* (7), 2549−2586.

(4) Sparks, D. L., Fundamentals of Soil Chemistry. *Encyclopedia of Water;* Science, Technology, and Society 2019, 1−11.

(5) Carabante, I.; Grahn, M.; Holmgren, A.; Kumpiene, J.; Hedlund, J. Adsorption of as (V) on Iron Oxide Nanoparticle Films Studied by in Situ Atr-Ftir Spectroscopy. *Colloids Surf., A* **2009**, *346* (1), 106−113.

(6) Hiemstra, T.; Zhao, W. Reactivity of Ferrihydrite and Ferritin in Relation to Surface Structure, Size, and Nanoparticle Formation Studied for Phosphate and Arsenate. *Environmental Science: Nano* **2016**, 3 (6), 1265−1279.

(7) Sposito, G. *The Chemistry of Soils*; Oxford University Press: New York,, 1987.

(8) Namayandeh, A.; Kabengi, N. Calorimetric Study of the Influence of Aluminum Substitution in Ferrihydrite on Sulfate Adsorption and Reversibility. *J. Colloid Interface Sci.* **2019**, *540*, 20−29.

(9) ThomasArrigo, L. K.; Kaegi, R.; Kretzschmar, R. Ferrihydrite Growth and Transformation in the Presence of Ferrous Iron and Model Organic Ligands. *Environ. Sci. Technol.* **2019**, *53* (23), 13636−13647.

(10) Soltis, J. A.; Feinberg, J. M.; Gilbert, B.; Penn, R. L. Phase Transformation and Particle-Mediated Growth in the Formation of Hematite from 2-Line Ferrihydrite. *Cryst. Growth Des.* **2016**, *16* (2), 922−932.

(11) Bolanz, R. M.; Bläss, U.; Ackermann, S.; Ciobotă, V.; Rösch, P.; Tarcea, N.; Popp, J.; Majzlan, J. The Effect of Antimonate, Arsenate, and Phosphate on the Transformation of Ferrihydrite to Goethite, Hematite, Feroxyhyte, and Tripuhyite. *Clays Clay Miner.* **2013**, *61* (1), 11−25.

(12) Das, S.; Hendry, M. J.; Essilfie-Dughan, J. Transformation of Two-Line Ferrihydrite to Goethite and Hematite as a Function of Ph and Temperature. *Environ. Sci. Technol.* **2011**, *45* (1), 268−275.

(13) Cudennec, Y.; Lecerf, A. The Transformation of Ferrihydrite into Goethite or Hematite, Revisited. *J. Solid State Chem.* **2006**, *179* (3), 716−722.

(14) Schwertmann, U.; Stanjek, H.; Becher, H. H. Long-Term in Vitro Transformation of 2-Line Ferrihydrite to Goethite/Hematite at 4, 10, 15 and 25°C. *Clay Minerals* **2004**, *39* (4), 433−438.

(15) Johnston, J. H.; Lewis, D. G. A Detailed Study of the Transformation of Ferrihydrite to Hematite in an Aqueous Medium at 92°C. *Geochim. Cosmochim. Acta* **1983**, *47* (11), 1823−1831.

(16) Burleson, D. J.; Penn, R. L. Two-Step Growth of Goethite from Ferrihydrite. *Langmuir* **2006**, *22* (1), 402−409.

(17) Burrows, N. D.; Hale, C. R. H.; Penn, R. L. Effect of Ph on the Kinetics of Crystal Growth by Oriented Aggregation. *Cryst. Growth Des.* **2013**, *13* (8), 3396−3403.

(18) Han, J.; Kim, M.; Ro, H.-M. J. E. C. L. Factors Modifying the Structural Configuration of Oxyanions and Organic Acids Adsorbed on Iron (Hydr) Oxides in Soils. A Review. *Environmental Chemistry Letters* **2020**, *18* (3), 631−662.

(19) Wurtsbaugh, W. A.; Paerl, H. W.; Dodds, W. K. Nutrients, Eutrophication and Harmful Algal Blooms Along the Freshwater to Marine Continuum. *Wires Water* **2019**, *6* (5), No. e1373.

(20) Sherris, A. R.; Baiocchi, M.; Fendorf, S.; Luby, S. P.; Yang, W.; Shaw, G. M. Nitrate in Drinking Water During Pregnancy and Spontaneous Preterm Birth: A Retrospective within-Mother Analysis in California. *Environ. Health Perspect.* **2021**, *129* (5), 57001.

(21) Mackay, A. In Some Aspects of the Topochemistry of the Iron Oxides and Hydroxides, Reactivity of solids: *Proceedings of the fourth international symposium on the reactivity of solids*, 1960; pp 571−583.

(22) Soltis, J. A.; Penn, R. L. Oriented Attachment and Nonclassical Formation in Iron Oxides. *Iron Oxides* **2016**, 243−268, DOI: 10.1002/9783527691395.ch11.

(23) Li, D.; Nielsen, M. H.; Lee, J. R. I.; Frandsen, C.; Banfield, J. F.; De Yoreo, J. J. Direction-Specific Interactions Control Crystal Growth by Oriented Attachment. *Science* **2012**, *336* (6084), 1014−1018.

(24) Zhu, G.; Sushko, M. L.; Loring, J. S.; Legg, B. A.; Song, M.; Soltis, J. A.; Huang, X.; Rosso, K. M.; De Yoreo, J. J. J. N. Self-Similar Mesocrystals Form Via Interface-Driven Nucleation and Assembly. *Nature* **2021**, *590* (7846), 416−422.

(25) Yuwono, V. M.; Burrows, N. D.; Soltis, J. A.; Anh Do, T.; Lee Penn, R. Aggregation of Ferrihydrite Nanoparticles in Aqueous Systems. *Faraday Discuss.* **2012**, *159* (1), 235−245.

(26) Namayandeh, A.; Borkiewicz, O. J.; Bompoti, N. M.; Chrysochoou, M.; Michel, F. M. Oxyanion Surface Complexes Control the Kinetics and Pathway of Ferrihydrite Transformation to Goethite and Hematite. *Environ. Sci. Technol.* **2022**, *56* (22), 15672−15684.

(27) Namayandeh, A.; Borkiewicz, O. J.; Bompoti, N. M.; Watson, S. K.; Kubicki, J. D.; Chrysochoou, M.; Michel, F. M. Effects of Oxyanion Surface Loading on the Rate and Pathway of Ferrihydrite Transformation. *ACS Earth and Space Chemistry* **2023**, *7* (10), 2154−2165.

(28) Banfield, J. F.; Welch, S. A.; Zhang, H.; Ebert, T. T.; Penn, R. L. Aggregation-Based Crystal Growth and Microstructure Development

in Natural Iron Oxyhydroxide Biomineralization Products. *Science* **2000**, *289* (5480), 751−754.
(29) Lee Penn, R.; Erbs, J. J.; Gulliver, D. M. Controlled Growth of Alpha-Feooh Nanorods by Exploiting-Oriented Aggregation. *J. Cryst. Growth* **2006**, *293* (1), 1−4.
(30) Lee Penn, R.; Tanaka, K.; Erbs, J. Size Dependent Kinetics of Oriented Aggregation. *J. Cryst. Growth* **2007**, *309* (1), 97−102.
(31) Yuwono, V. M.; Burrows, N. D.; Soltis, J. A.; Penn, R. L. Oriented Aggregation: Formation and Transformation of Mesocrystal Intermediates Revealed. *J. Am. Chem. Soc.* **2010**, *132* (7), 2163−2165.
(32) Burrows, N. D.; Hale, C. R. H.; Penn, R. L. Effect of Ionic Strength on the Kinetics of Crystal Growth by Oriented Aggregation. *Cryst. Growth Des.* **2012**, *12* (10), 4787−4797.
(33) Chen, S. A.; Heaney, P. J.; Post, J. E.; Eng, P. J.; Stubbs, J. E. Hematite-Goethite Ratios at Ph 2−13 and 25−170 °C: A Time-Resolved Synchrotron X-Ray Diffraction Study. *Chem. Geol.* **2022**, *606*, No. 120995.
(34) Michel, F. M., Total Scattering Studies of Natural and Synthetic Ferrihydrite. In *Advanced Applications of Synchrotron Radiation in Clay Science*; Clay Minerals Society: 2014; Vol. *19*, p 0.
(35) Liao, S.; Wang, X.; Yin, H.; Post, J. E.; Yan, Y.; Tan, W.; Huang, Q.; Liu, F.; Feng, X. Effects of Al Substitution on Local Structure and Morphology of Lepidocrocite and Its Phosphate Adsorption Kinetics. *Geochim. Cosmochim. Acta* **2020**, *276*, 109−121.
(36) Gu, C.; Wang, Z.; Kubicki, J. D.; Wang, X.; Zhu, M. X-Ray Absorption Spectroscopic Quantification and Speciation Modeling of Sulfate Adsorption on Ferrihydrite Surfaces. *Environ. Sci. Technol.* **2016**, *50* (15), 8067−8076.
(37) Antelo, J.; Arce, F.; Fiol, S. Arsenate and Phosphate Adsorption on Ferrihydrite Nanoparticles. Synergetic Interaction with Calcium Ions. *Chem. Geol.* **2015**, *410*, 53−62.
(38) Curtin, D.; Campbell, C. A.; Jalil, A. Effects of Acidity on Mineralization: Ph-Dependence of Organic Matter Mineralization in Weakly Acidic Soils. *Soil Biology and Biochemistry* **1998**, *30* (1), 57−64.
(39) Lu, H. l.; Li, K. w.; Nkoh, J. N.; He, X.; Xu, R. k.; Qian, W.; Shi, R. y.; Hong, Z. n. Effects of Ph Variations Caused by Redox Reactions and Ph Buffering Capacity on Cd(Ii) Speciation in Paddy Soils During Submerging/Draining Alternation. *Ecotoxicol. Environ. Saf.* **2022**, *234*, No. 113409.
(40) Kjøller, C.; Postma, D.; Larsen, F. Groundwater Acidification and the Mobilization of Trace Metals in a Sandy Aquifer. *Environ. Sci. Technol.* **2004**, *38* (10), 2829−2835.
(41) Yang, X.; Juhas, P.; Farrow, C. L.; Billinge, S. J. Xpdfsuite: An End-to-End Software Solution for High Throughput Pair Distribution Function Transformation, Visualization and Analysis. *arXiv: Materials Science* **2014**, DOI: 10.48550/arXiv.1402.3163.
(42) Ressler, T. Winxas: A Program for X-Ray Absorption Spectroscopy Data Analysis under Ms-Windows. *Journal of Synchrotron Radiation* **1998**, *5* (2), 118−122.
(43) Sposito, G. *The Chemistry of Soils*. 2nd ed ed.; Oxford University Press: Oxford, 2008.
(44) Harvey, O. R.; Rhue, R. D. Kinetics and Energetics of Phosphate Sorption in a Multi-Component Al(Iii)−Fe(Iii) Hydr-(Oxide) Sorbent System. *J. Colloid Interface Sci.* **2008**, *322* (2), 384−393.
(45) Geelhoed, J. S.; Hiemstra, T.; Van Riemsdijk, W. H. Phosphate and Sulfate Adsorption on Goethite: Single Anion and Competitive Adsorption. *Geochim. Cosmochim. Acta* **1997**, *61* (12), 2389−2396.
(46) Gálvez, N.; Barrón, V.; Torrent, J. Effect of Phosphate on the Crystallization of Hematite, Goethite, and Lepidocrocite from Ferrihydrite. *Clays and Clay Minerals* **1999**, *47* (3), 304−311.
(47) Arai, Y.; Sparks, D. L. Atr−Ftir Spectroscopic Investigation on Phosphate Adsorption Mechanisms at the Ferrihydrite−Water Interface. *J. Colloid Interface Sci.* **2001**, *241* (2), 317−326.
(48) Hongshao, Z.; Stanforth, R. J. E. S. Technology, Competitive Adsorption of Phosphate and Arsenate on Goethite. *Environ. Sci. Technol.* **2001**, *35* (24), 4753−4757, DOI: 10.1021/es010890y.
(49) Kubicki, J. D.; Kwon, K. D.; Paul, K. W.; Sparks, D. L. Surface Complex Structures Modelled with Quantum Chemical Calculations: Carbonate, Phosphate, Sulphate, Arsenate and Arsenite. *European Journal of Soil Science* **2007**, *58*, 932.
(50) Zhang, X.; Yao, H.; Lei, X.; Lian, Q.; Roy, A.; Doucet, D.; Yan, H.; Zappi, M. E.; Gang, D. D. A Comparative Study for Phosphate Adsorption on Amorphous Feooh and Goethite (A-Feooh): An Investigation of Relationship between the Surface Chemistry and Structure. *Environmental Research* **2021**, *199*, No. 111223.
(51) Arroyave, J. M.; Avena, M.; Tan, W.; Wang, M. The Two-Species Phosphate Adsorption Kinetics on Goethite. *Chemosphere* **2022**, *307*, No. 135782.
(52) Sverjensky, D. A.; Fukushi, K. Anion Adsorption on Oxide Surfaces: Inclusion of the Water Dipole in Modeling the Electrostatics of Ligand Exchange. *Environ. Sci. Technol.* **2006**, *40* (1), 263.
(53) Sverjensky, D. A.; Fukushi, K. A Predictive Model (Etlm) for as(Iii) Adsorption and Surface Speciation on Oxides Consistent with Spectroscopic Data. *Geochim. Cosmochim. Acta* **2006**, *70* (15), 3778−3802.
(54) Fukushi, K.; Sverjensky, D. A. A Surface Complexation Model for Sulfate and Selenate on Iron Oxides Consistent with Spectroscopic and Theoretical Molecular Evidence. *Geochim. Cosmochim. Acta* **2007**, *71* (1), 1.
(55) Langmuir, D. *Aqueous Environmental*; Prentice Hall: 1997.
(56) Penn, R. L.; Banfield, J. F. Imperfect Oriented Attachment: Dislocation Generation in Defect-Free Nanocrystals. *Science* **1998**, *281* (5379), 969−971.
(57) Stemig, A. M.; Do, T. A.; Yuwono, V. M.; Arnold, W. A.; Penn, R. L. Goethite Nanoparticle Aggregation: Effects of Buffers, Metal Ions, and 4-Chloronitrobenzene Reduction. *Environmental Science: Nano* **2014**, *1* (5), 478−487.
(58) Bilardello, D.; Banerjee, S. K.; Volk, M. W. R.; Soltis, J. A.; Penn, R. L. Simulation of Natural Iron Oxide Alteration in Soil: Conversion of Synthetic Ferrihydrite to Hematite without Artificial Dopants, Observed with Magnetic Methods. *Geochem. Geophys. Geosyst.* **2020**, *21* (7), No. e2020GC009037.
(59) Cornell, R. M.; Giovanoli, R. Effect of Solution Conditions on the Proportion and Morphology of Goethite Formed from Ferrihydrite. *Clays and Clay Minerals* **1985**, *33* (5), 424−432.
(60) Fournier, J. A.; Carpenter, W.; De Marco, L.; Tokmakoff, A. Interplay of Ion−Water and Water−Water Interactions within the Hydration Shells of Nitrate and Carbonate Directly Probed with 2d Ir Spectroscopy. *J. Am. Chem. Soc.* **2016**, *138* (30), 9634−9645.
(61) Loganathan, P.; Vigneswaran, S.; Kandasamy, J. Enhanced Removal of Nitrate from Water Using Surface Modification of Adsorbents − a Review. *Journal of Environmental Management* **2013**, *131*, 363−374.
(62) Spagnoli, D.; Gilbert, B.; Waychunas, G. A.; Banfield, J. F. Prediction of the Effects of Size and Morphology on the Structure of Water around Hematite Nanoparticles. *Geochim. Cosmochim. Acta* **2009**, *73* (14), 4023−4033.
(63) Torrent, J.; Guzman, R. Crystallization of Fe(Iii)-Oxides from Ferrihydrite in Salt Solutions: Osmotic and Specific Ion Effects. *Clay Minerals* **1982**, *17* (4), 463−469.
(64) Derjaguin, B. V.; Landau, L. D. Theory of the Stability of Strongly Charged Lyophobic Sols and of the Adhesion of Strongly Charged Particles in Solutions of Electrolytes. *Acta Physicochim. URSS* **1941**, *14*, 633−662.
(65) Vazirzadeh, A.; Jafarifard, K.; Ajdari, A.; Chisti, Y. Removal of Nitrate and Phosphate from Simulated Agricultural Runoff Water by Chlorella Vulgaris. *Science of The Total Environment* **2022**, *802*, No. 149988.
(66) Wang, X.; Olsen, L. M.; Reitan, K. I.; Olsen, Y. Discharge of Nutrient Wastes from Salmon Farms: Environmental Effects, and Potential for Integrated Multi-Trophic Aquaculture. *Aquaculture Environment Interactions* **2012**, *2* (3), 267−283.
(67) Wang, Xiaoming; Liu, Fan; Tan, Wenfeng; Li, Wei; Feng, Xionghan; Sparks, D. L., Characteristics of Phosphate Adsorption-

Desorption onto Ferrihydrite: Comparison with Well-Crystalline Fe (Hydr)Oxides. 2013, *178* (1), 1−11.
(68) Sassi, M.; Rosso, K. M. Ab Initio Evaluation of Solid-State Transformation Pathways from Ferrihydrite to Goethite. *ACS Earth and Space Chemistry* **2022**, *6* (3), 800−809.
(69) Das, S.; Hendry, M. J.; Essilfie-Dughan, J. Effects of Adsorbed Arsenate on the Rate of Transformation of 2-Line Ferrihydrite at Ph 10. *Environ. Sci. Technol.* **2011**, *45* (13), 5557−5563.

https://doi.org/10.1021/acs.est.3c09955
Environ. Sci. Technol. 2024, 58, 5952−5962